

STRESS DUE TO INTERFACIAL SLIP CAUSING SLEEVE FRACTURE IN SHRINK-FITTED WORK ROLL*

NAO-AKI NODA[†], RAHIMAH ABDUL RAFAR, YOSHIKAZU SANO

Department of Mechanical Engineering, Kyushu Institute of Technology, 1-1 Sensui-cho,

Tobata-ku, Kitakyushu-shi 804-8550, Japan

noda.naoaki844@mail.kyutech.jp

Received Day Month Day

Revised Day Month Day

The rolls are classified into two types; one is a single-solid type, and the other is a shrink-fitted construction type consisting of a sleeve and a shaft. The bimetallic work rolls are widely used in the roughing stands of hot rolling stand mills. Regarding a shrink-fitted construction type, the interfacial slip sometimes appears between the shaft and the shrink-fitted sleeve. This interfacial slip can be regarded as the relative displacement between the sleeve and the shaft. In this paper, the stress due to the interfacial slip is studied because the stress may cause the sleeve fracture. It is found that the stress in the shrink-fitted surface is slightly decreased with increasing number of rotations n . Therefore, the stress obtained by the simulation at $n=2$ can be used to estimate the fatigue strength.

Keywords: Shrink-fitting; rolling roll; bimetallic roll; interfacial slip; motor torque; sleeve; shaft.

1. Introduction

Rolling rolls are essential to the iron and steel industries, and therefore lots of efforts have been done to improve their mechanical properties. Fig. 1 illustrates the rolling roll in roughing stands of hot rolling stand mills. The rolls are classified into two types; one is a single-solid type, and the other is a shrink-fitted assembled type consisting of a sleeve and a shaft. In shrink-fitted sleeve roll, although the wear and surface roughness soon appear on the roll body, the shaft can be reused. However, it is clarified in the previous study that this shrink-fitted structure has generated the interfacial slip between the sleeve and the shaft.¹⁻³ Furthermore, in order to consider the roll breakage caused by the stress due to the interfacial slip, the stress state in the shrink-fitted surface will be focused in this paper.

*For the title, try not to use more than 3 lines. Typeset the title in 10 pt Times Roman, uppercase and boldface.

[†]Department of Mechanical Engineering, Kyushu Institute of Technology, 1-1 Sensui-cho, Kitakyushu-shi, 804-8550 Japan.

2. Numerical simulation method of interface slip under the action of shaft drive torque

Fig. 1 illustrates two-dimensional modelling in numerical simulation. Fig. 1a illustrates the central cross section of real roll and Fig. 1b illustrates the real roll by shifting the load on the roll surface with the roll center fixed. Here, the motor torque T is balanced with the frictional moment S as $T = SD/2$ where D is the sleeve outer diameter. Fig. 1c shows the analysis roll model that is used in the study. In Fig. 1, the roll is subjected to compressive force P from the back-up roll, the rolling reaction force P_h , the frictional force S from the strip, the bending force P_b from the bearing and torque T from the motor. Since two-dimensional model is applied, the external force per unit length should be considered. The loading condition used in this study is the concentrated loading P from the back-up roll and the reaction P from the strip with $P = 13270$ N/mm. Here, when the

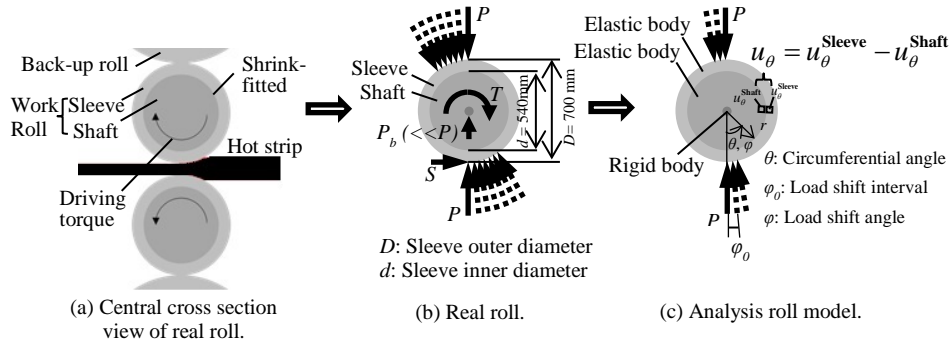


Fig. 1. Modelling and simulation for interfacial slip when P is the load from back-up roll and hot-strip, S is the frictional force, P_b is the bending force from bearing, T is the driving torque.

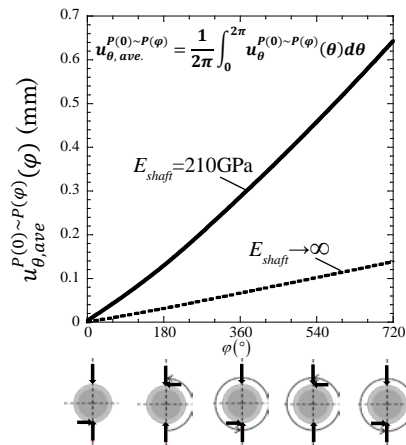


Fig. 2. Interfacial displacement for shaft Young's modulus $E_{shaft} = 210$ GPa in comparison with $E_{shaft} \rightarrow \infty$.

rated torque of the motor is $T_m = 471$ Nm/mm, the frictional force can be calculated as $S = 1346$ Nm/mm. The shrink-fitting ratio is defined as δ/d , where δ is the diameter difference between the inner diameter of the sleeve and d is the sleeve inner diameter. In this study, $\delta/d = 0.5 \times 10^{-3}$ is used with the friction coefficient $\mu = 0.3$ between the sleeve and the shaft.

In this analysis, the circumferential relative displacement at the interface between the sleeve and shaft when load move from the angle $\varphi = 0^\circ$ to $\varphi = \varphi$ is defined as $u_{\theta}^{P(0) \sim P(\varphi)}$. Here, notation φ denotes the load shifting angle and θ denotes the position where the displacement is evaluated. Thus, the accumulation of the displacement is given by the Eq. 1.

$$u_{\theta,ave}^{P(0) \sim P(\varphi)} = \frac{1}{2\pi} \int_0^{2\pi} u_{\theta}^{P(0) \sim P(\varphi)}(\theta) d\theta \quad (1)$$

Fig. 2 shows the interfacial displacement $u_{\theta,ave}^{P(0) \sim P(\varphi)}$ by rotating the load twice for shaft Young's modulus $E_{shaft} \rightarrow \infty$ and $E_{shaft} = 210$ GPa. From the figure, the amount of interfacial slip $u_{\theta,ave}^{P(0) \sim P(\varphi)}$ increases almost linearly with increasing the load shift angle φ . The interface slip may occur as soon as the load shifting starts.

3. Stress on the inner surface of the sleeve

In the sleeve assembly type roll, it should be noted that the circumferential slippage sometimes occurs even though the resistance torque at the interface is larger than the motor torque. Due to this slip, a localized adhesion occurs and causes a crack initiation. Then, the crack propagates and form a groove-like flaw. The repeated stress concentration at this flaw increases the flaw dimension and finally cause sleeve fracture.⁴ In this way, the stress σ_{θ} appearing at the shrink-fitted surface should be estimated since

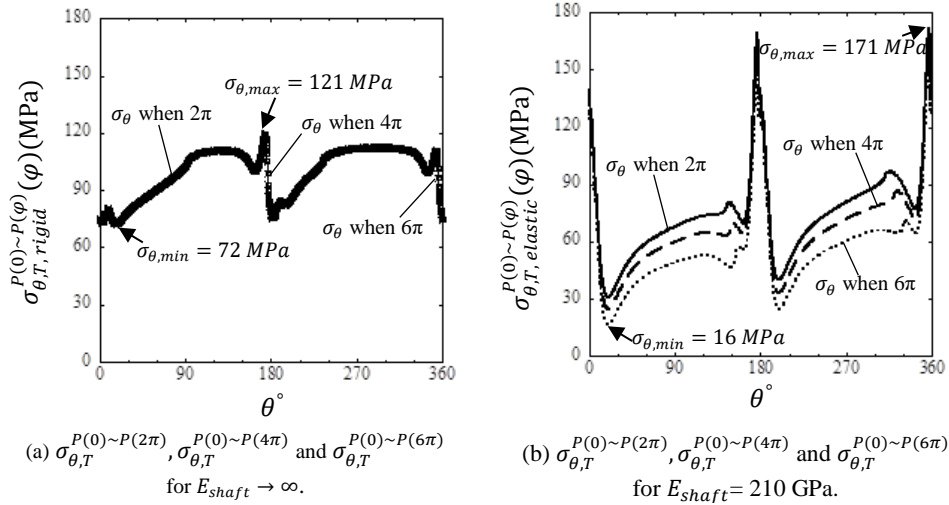


Fig. 3. $\sigma_{\theta,T}^{P(0) \sim P(2\pi)}$, $\sigma_{\theta,T}^{P(0) \sim P(4\pi)}$ and $\sigma_{\theta,T}^{P(0) \sim P(6\pi)}$ when number of rotations $n = 1, 2$ and 3 of $E_{shaft} \rightarrow \infty$ and $E_{shaft} = 210$ GPa.

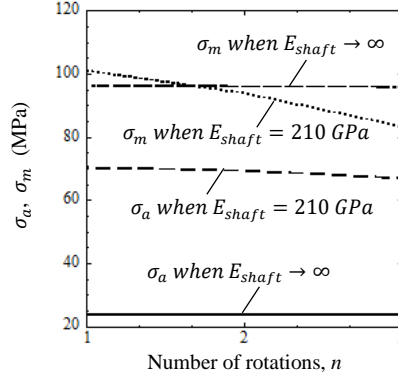


Fig. 4. Stress amplitude σ_a and mean stress σ_m for $E_{shaft}=210$ GPa in comparison with $E_{shaft} \rightarrow \infty$.

σ_θ is the largest stress component and causes such damage.

Fig. 3 shows the stress distribution $\sigma_{\theta,T}^{P(0)\sim P(2\pi)}$, $\sigma_{\theta,T}^{P(0)\sim P(4\pi)}$ and $\sigma_{\theta,T}^{P(0)\sim P(6\pi)}$ when the number of rotations $n=1, 2$ and 3 , respectively, for (a) $E_{shaft} \rightarrow \infty$ and (b) $E_{shaft}=210$ GPa. In Fig. 3a, there is almost no difference in the stress distribution σ_θ when $n=1, 2$ and 3 . From Fig. 3a, the maximum stress is $\sigma_{\theta,max}=121$ MPa and the minimum stress is $\sigma_{\theta,min}=72$ MPa. In Fig. 3b, the interfacial stress obtained shows differences in the stress distribution when $n=1, 2$ and 3 . From Fig. 3b, the maximum stress is $\sigma_{\theta,max}=171$ MPa and the minimum stress is $\sigma_{\theta,min}=16$ MPa. Regarding the possibility of fatigue fracture from the inner surface of the sleeve due to these stresses, it is known that the inevitable tensile residual stress has a large effect on the inner surface of the sleeve.

The stress amplitude at which failure occurs for a given number of rotations is simplified in Fig. 4. In Fig. 4, stress amplitude σ_a and mean stress σ_m for $E_{shaft} \rightarrow \infty$ shows almost constant values as n increases. As for $E_{shaft}=210$ GPa, the fatigue strength shows the safety variation because stress amplitude σ_a and mean stress σ_m decreasing as the number of rotations increases.

4. Conclusion

In this paper, the stress due to the interfacial slip is studied because the stress may cause the sleeve fracture. In this study, the circumferential stress σ_θ should be estimated since σ_θ is the largest stress component and may cause sleeve damage. From the analysis, it was found that the stress in the shrink-fitted surface for $E_{shaft} \rightarrow \infty$ shows almost constant values as the number of rotations n increases. As for $E_{shaft}=210$ GPa, the stress in the shrink-fitted surface is slightly decreased with increasing n . Therefore, the stress obtained by simulation at $n=2$ can be used to estimate the fatigue strength.

References

1. H. Sakai, N.A. Noda, Y. Sano, G. Zhang, and Y. Takase, *Tetsu-to-Hagane* **105**, 1126 (2019).
2. H. Sakai, N.A. Noda, Y. Sano, G. Zhang, and Y. Takase, *Tetsu-to-Hagane* **105**, 411 (2019).
3. H. Sakai, N.A. Noda, Y. Sano, G. Zhang, and Y. Takase, *ISIJ Int.* **59**, 889 (2019).
4. E. Matsunaga, T. Tsuyuki, and Y. Sano, *CAMP-ISIJ* **11**, 362 (1998).